Chin. J. Astron. Astrophys. Vol. 3 (2003), No. 3, 225–234
(*http://www.chjaa.org* or *http://chjaa.bao.ac.cn*)

Chinese Journal of Astronomy and Astrophysics

Cylindrical Jet – Wind Interaction Model of Gamma-Ray Burst Afterglows *

Hai-Tao Ma, Yong-Feng Huang, Zi-Gao Dai and Tan Lu

Department of Astronomy, Nanjing University, Nanjing 210093; hyf@nju.edu.cn

Received 2003 January 19; accepted 2003 April 7

Abstract Observations on relativistic jets in radio galaxies, active galactic nuclei, and "microquasars" revealed that many of these outflows are cylindrical, not conical. So it is worthwhile to investigate the evolution of cylindrical jets in gamma-ray bursts. We discuss afterglows from cylindrical jets in a wind environment. Numerical results as well as analytic solutions in some special cases are presented. Our light curves are steeper compared to those in the homogeneous interstellar medium case, carefully considered by Cheng, Huang & Lu. We conclude that some afterglows, used to be interpreted as isotropic fireballs in a wind environment, can be fitted as well by cylindrical jets interacting with a wind.

Key words: gamma-rays: bursts — ISM: jets and outflows — radiation mechanisms: non-thermal — stars: neutron

1 INTRODUCTION

The fireball model for gamma-ray bursts (GRBs) leads to predictions of the afterglow emission (Katz 1994; Mészáros & Rees 1997). Before the GRB prompt phase, baryons in the fireball are accelerated to ultra-relativistic speeds by the huge radiation pressure, but shocks will reconvert the kinetic energy of the baryons into nonthermal particles and photon energy (Wu et al. 2001). The internal shock model is generally regarded as the most attractive model for the prompt γ-ray emission of classical GRBs. Zhang & Mészáros (2002) have compared various models by means of predictions of the narrowness of the spectral breaking energy, $E_{\rm p}$, through a simple Monte-Carlo simulation. The subsequent afterglows will occur after the swept-up mass equals γ^{-1} of the initial ejecta mass (Rees & Mészáros 1992; Mao & Wang 2001a, b; Huang, Yang & Lu 2001; Cheng & Lu 2001), where γ is the bulk Lorentz factor. In February of 1997 the Italian-Dutch satellite BeppoSAX discovered an X-ray counterpart to GRB 970228 (Sahu et al. 1997; van Paradijs et al. 1997). Since then 41 X-ray afterglows and 36 optical afterglows have so far been detected (see the web page "http://www.mpe.mpg.de/∼jcg/grbgen.html"). The majority of the optical afterglows yielded redshifts, which makes it clear that GRBs originate from cosmological distances.

∗ Supported by the National Natural Science Foundation of China.

A hot issue in the GRB field is whether a GRB is produced from an isotropic fireball or a highly collimated jet (Rhoads 1997). The afterglow of GRB 970508 was characterized by a break in its light curve, and such breaks were observed later in other afterglows, such as GRBs 990510, 990123, and 000301. For a conical jet with half opening angle θ, it is believed that due to both the edge effect and the lateral expansion effect, a break will appear in the light curve when the bulk Lorentz factor γ drops below θ^{-1}. Huang et al. (1999a, b) used their improved dynamical model and found that the most obvious light curve break occurs at the relativistic-Newtonian transition point. Observation of GRB 990123 indicates an inconceivable isotropic energy of 10^{54} erg (Akerlof et al. 1999), and a jet geometry may need to be introduced to abate the energy crisis. To produce polarized emission some asymmetry is also required. Observation on the polarization of afterglows may give us a very powerful tool to find out the degree of collimation of the GRB ejecta, and hence the true total emitted power (Ghisellini 2001).

The environment of the GRBs is another fundamental problem. A massive star origin for GRBs implies a stellar wind environment, while GRBs produced by the merger of compact objects occur in the homogeneous interstellar medium (ISM). The optical afterglow is generally expected to decline more steeply in the wind case than in the uniform ISM case, but this effect may be masked by variations in the electron spectral index. Optical flashes of GRBs may provide a good diagnosis of the environment (Kobayashi & Zhang 2003; Chevalier & Li 2000).

More and more observations on relativistic jets in radio galaxies, active galactic nuclei (AGN), and "microquasars" in the Galaxy have revealed that the outflows are usually cylindrical, not conical (Perley, Bridle & Willis 1984; Biretta, Sparks & Macchetto 1999). It is worthwhile to discuss the possibility of GRBs originating from cylindrical jets, though the collimation mechanism is still unclear. Cheng, Huang & Lu (2001, hereafter CHL) has considered a cylindrical jet expanding in the ISM. They found that the light curves of cylindrical jets turn flatter after the relativistic-Newtonian transition point, whether or not lateral expansion takes place. It is suggested that some afterglows decaying as $t^{-1.1}$ — $t^{-1.3}$ may be due to cylindrical jets, rather than isotropic fireballs (Huang et al. 2002). In this letter we study the evolution of a cylindrical jet propagating into a stellar wind environment, i.e., where the density of the surrounding medium $n(R) \propto R^{-2}$.

2 MODEL

2.1 Wind Density

Recent evidence has given support to the idea that long-duration γ-ray bursts result from the collapse of massive stars in very energetic supernova-like explosions (MacFadyen, Woosley & Heger 2001). Dai & Lu (1998) assumed that the density of the surrounding medium followed a power law, i.e., $n \propto R^{-k}$, and they found they could well fit the X-band afterglow of GRB 970616 by assuming $k = 2$, which supports the massive star origin. Chevalier & Li (1999, hereafter CL) considered the case of Wolf-Rayet stars with initial masses more than $25M_{\odot}$ losing their H envelopes in winds. For the Wolf-Rayet stars, typical wind-loss rate is $\dot{M} \approx 10^{-5} - 10^{-4} M_{\odot}$ yr^{-1}, and typical wind speed is $V_{\rm w} \approx 1000 - 25000$ km s^{-1} (Willis 1991). Clearly the low wind velocity would lead to a higher circumstellar density. CL also mentioned that if a burst occurred in a red supergiant star, then $V_{\rm w} \approx 10\,{\rm km\ s^{-1}}$. Assuming $n(R) = AR^{-2}$, and with $4\pi R^2 n m_{\rm p} V_{\rm w} = \dot{M}$, we can easily obtain

$$A = \frac{1}{4\pi}\frac{\dot{M}}{m_{\rm p} V_{\rm w}} = 3.0 \times 10^{38}\ A_*\ \ {\rm cm^{-1}}\ , \tag{1}$$

$$A_* = \frac{\dot{M}\ /10^{-4}\,M_\odot \mathrm{yr}^{-1}}{V_\mathrm{w}/10\,\mathrm{km\ s}^{-1}}\ , \tag{2}$$

where m_p is the mass of proton. The wind scale is another important point. CL estimated the position of the wind termination shock to be 5×10^{18} cm for Wolf-Rayet stars, then the density increases by a factor of 4 and becomes approximately constant at larger radii.

2.2 Dynamics and Synchrotron Radiation

To depict the expansion of GRB remnants, Huang et al. (1999a, b) proposed a refined equation,

$$\frac{\mathrm{d}\gamma}{\mathrm{d}m} = -\frac{\gamma^2-1}{M_\mathrm{ej}+\epsilon m+2(1-\epsilon)\gamma m}, \tag{3}$$

where m is the rest mass of the swept-up medium, M_ej is the initial ejecta mass and ϵ is the radiative efficiency. Figure 1 is drawn to compare Huang's equation with the foregoing equation which is correct only for the relativistic phase. From Fig. 1 we can see that Eq. (3) works not only in the relativistic phase, but also in the non-relativistic phase. Huang et al. (1999a, b) have also shown that Eq. (3) is correct for both highly radiative shocks (ϵ=1) and adiabatic shocks (ϵ=0). For simplicity, we will only consider the adiabatic case.

Referring to the equations in Huang et al. (2000a, b, c) which describe conical jets and the equations in CHL which describe cylindrical jets in the ISM environment, we can deduce dynamic equations in the case of cylindrical jet propagating into the wind circumstance.

We use eqs. (3)–(5) in CHL to describe the evolution of the radius (R), the swept-up mass (m) and the lateral radius (a). Note that the density here is not constant, but scales as $n\propto R^{-2}$. Combining these equations, we can program the dynamical evolution of cylindrical jets. In the next section, we will present our numerical results.

In the absence of radiation loss, the distribution of the shock accelerated electrons behind the blast wave is usually assumed to be a power law function of the electron energy (Huang et al. 1998),

$$\frac{\mathrm{d}N'_\mathrm{e}}{\mathrm{d}\gamma_\mathrm{e}} \propto \gamma_\mathrm{e}^{-p}, \quad (\gamma_\mathrm{e,min}\le\gamma_\mathrm{e}\le\gamma_\mathrm{e,max}), \tag{4}$$

where p is an index which usually varies between 2 and 3. As usual, we assume that the magnetic energy density in the co-moving frame is a fraction ξ_B^2 of the total thermal energy density ($B'^2/8\pi=\xi_\mathrm{B}^2 e'$), and that electrons carry a fraction ξ_e of the proton energy. Then the maximum Lorentz factor of the electrons is $\gamma_\mathrm{e,max}=10^8(B'/1\mathrm{G})^{-1/2}$ (Dai et al. 1998, 1999), and the minimum Lorentz factor is

$$\gamma_\mathrm{e,min}=\xi_\mathrm{e}(\gamma-1)\left(\frac{m_\mathrm{p}}{m_\mathrm{e}}\right)\left(\frac{p-2}{p-1}\right)+1, \tag{5}$$

where m_e is the electron mass. The equation for the cooling electron Lorentz factor, γ_c, is defined by the equality of its radiative cooling timescale with the dynamical timescale (Sari, Piran & Narayan 1998)

$$\gamma_\mathrm{c}=\frac{6\pi m_\mathrm{e}c}{\sigma_\mathrm{T}\gamma B'^2 t}, \tag{6}$$

where σ_T is the Thomson cross-section, t the time of the observation, and c the speed of light. Electrons with Lorentz factors below γ_c are adiabatic, and those above, highly radiative. The actual distribution that takes into account the synchrotron cooling effect should be given

according to Dai et al. (1999), then the synchrotron radiation can be calculated by using eqs. (8)–(13) in CHL.

3 ANALYTIC SOLUTION AND NUMERICAL RESULTS

We use the following initial values and parameters in our model: original ejecta mass $M_{\rm ej} = 2 \times 10^{-8} M_\odot$, initial Lorenz factor $\gamma_0 = 200$, hence, $m_0 = 1 \times 10^{-10} M_\odot$. We take $R_0 = 1 \times 10^{16}$ cm, $A = 3 \times 10^{38}$ cm^{-1}, and assume $a_0 = 0.05 R_0$ cm unless declared explicitly. In calculating the R-band flux densities, we take the luminosity distance $D_{\rm L} = 1$ Gpc, $p = 2.5$, $\xi_{\rm e} = 0.1$, $\xi_{\rm B}^2 = 10^{-6}$. Observers are assumed to be on the axis, so that the viewing angle is $\Theta = 0$. We define $v_\perp$ as the velocity of lateral expansion, and discuss the case where the cylindrical jet does not expand laterally and the case where it does so at the comoving sound speed.

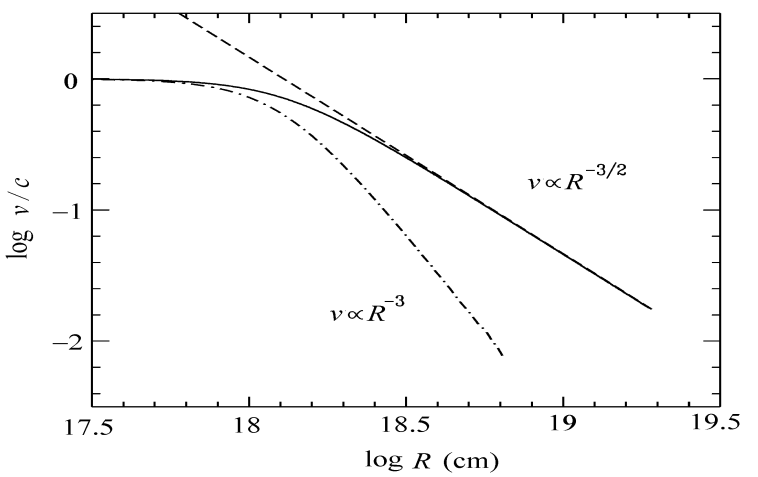

Fig. 1 Velocity vs. radius for an isotropic adiabatic fireball (Huang 2000). The dashed line is the familiar Sedov solution in the Newtonian phase. The dash-dotted line is only suitable in the relativistic phase. The solid line corresponds to the refined model (i.e., Eq. (3)), which is consistent with the Sedov solution.

3.1 The Case $v_\perp \equiv 0$

Solving our dynamical equations numerically, we show the evolution of the Lorentz factor of the shock in Fig. 2 and that of the radius in Fig. 3. From Fig. 2, we can see that a narrow jet without lateral expansion cannot decelerate into Newtonian phase because the particle density dilutes rapidly with radius, but the cross section remains constant. It is obvious that if $a \ll 0.005 R_0$ the cylindrical jet will traverse the wind region to the ISM region very quickly (see Fig. 3). When it expands into the ISM region, the case turns to what CHL has already depicted. Here, we only discuss the case where the cylindrical jet can decelerate into the Newtonian phase or a moderately relativistic phase, i.e. $\gamma < 10$, then it can evolve in the wind within a typical time of an afterglow observation.

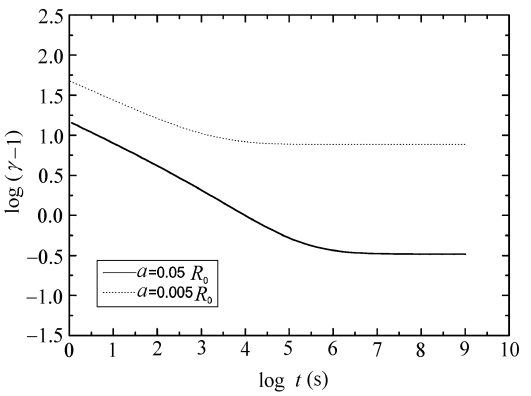

Fig. 2 Evolution of the Lorentz factor of the shock, γ, when $v_\perp \equiv 0$.

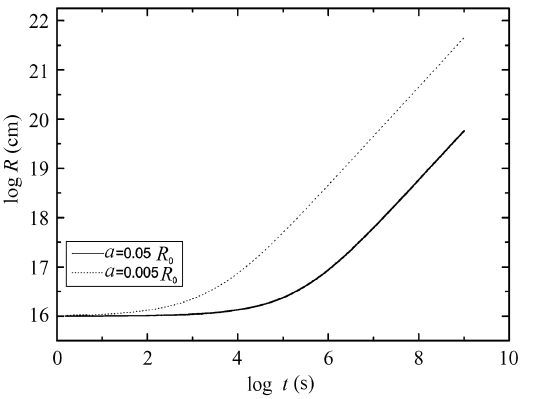

Fig. 3 Evolution of the radius, R, when $v_\perp \equiv 0$.

A cylindrical jet cannot decelerate noticeably when the particle numbers swept up at large radius is negligible. From Fig. 2, whether or not the jet decelerates into Newtonian phase, we can assume the Lorentz factor $\gamma \approx$ const. in later stage, then we have $m \approx$ const., $R \propto t$. Additionally, from the shock conditions (Blandford & McKee 1976; Huang et al. 1999a, b), the co-moving thermal energy density is

$$e' = \frac{\hat{\gamma}\gamma + 1}{\hat{\gamma} - 1}(\gamma - 1)AR^{-2}m_{\rm p}c^2, \tag{7}$$

which indicates $e' \propto R^{-2} \propto t^{-2}$, so we have $B' \propto (e')^{1/2} \propto t^{-1}$, and the cooling frequency $\nu_{\rm c} \propto \gamma\gamma_{\rm c}^2 B' \propto t$ (Sari et al. 1998). Since the peak frequency of synchrotron radiation is $\nu_{\rm m} \propto \gamma\gamma_{\rm e,\,min}^2 B'$ (Sari et al. 1998), we have $\nu_{\rm m} \propto t^{-1}$, and the peak flux density is $S_{\nu,\,\max} = N_e P_{\nu,\,\max}/\Omega D_{\rm L}^2 \propto N_{\rm e}\gamma B' \propto t^{-1}$, where $N_{\rm e}$ is the total number of electrons, Ω the solid angle, and $P_{\nu,\,\max}$ the peak power (Sari et al. 1998). Note that if the jet is still relativistic, the half opening radiative angle θ equals γ^{-1} due to the relativistic beaming effect. As $\Omega \propto \theta^2 \propto \gamma^{-2}$, $S_{\nu,\,\max} \propto N_{\rm e}\gamma B'/\gamma^{-2} \propto t^{-1}$ is adopted. At last, we can derive the flux density of the afterglow at sufficiently late stages as follows:

$$S_\nu \approx \begin{cases} S_{\nu,\,\max}\left(\frac{\nu}{\nu_{\rm m}}\right)^{-(p-1)/2} \propto \nu^{-(p-1)/2}t^{-(p+1)/2}, & (\nu_{\rm m} \le \nu < \nu_{\rm c},\ \text{slow cooling}), \\ S_{\nu,\,\max}\left(\frac{\nu_{\rm c}}{\nu_{\rm m}}\right)^{-(p-1)/2}\left(\frac{\nu}{\nu_{\rm c}}\right)^{-p/2} \propto \nu^{-p/2}t^{-p/2}, & (\nu_{\rm m} < \nu_{\rm c} \le \nu,\ \text{slow cooling}), \\ S_{\nu,\,\max}\left(\frac{\nu}{\nu_{\rm c}}\right)^{-1/2} \propto \nu^{-1/2}t^{-1/2}, & (\nu_{\rm c} \le \nu < \nu_{\rm m},\ \text{fast cooling}), \\ S_{\nu,\,\max}\left(\frac{\nu_{\rm m}}{\nu_{\rm c}}\right)^{-1/2}\left(\frac{\nu}{\nu_{\rm m}}\right)^{-p/2} \propto \nu^{-p/2}t^{-p/2}, & (\nu_{\rm c} < \nu_{\rm m} \le \nu,\ \text{fast cooling}). \end{cases} \tag{8}$$

Figure 4 illustrates the R-band afterglow light curves. The solid line represents a cylindrical jet which can decelerate into Newtonian phase, and its slope is -1.70; the dotted line represents

a cylindrical jet which cannot enter into Newtonian phase, and its slope is -1.74. It is clearly shown in Fig. 5 that $\nu_{\rm m} \leq \nu_{\rm R} < \nu_{\rm c}$ is satisfied after tens of seconds, and we can see they are both in good agreement with our analytical result of -1.75. Note that the earlier light curve break in Fig. 4 is produced by initial value effect, not by dynamics effect. Figure 6 illustrates the impact of three other parameters, $\xi_{\rm e}$, $\xi_{\rm B}^2$ and Θ, on the light curve. Generally, $\xi_{\rm e}$ and $\xi_{\rm B}^2$ do not change the slope of the light curve. In the Θ=0.1 case, the flux density does not decrease as markedly as in the ISM case (CHL), which means that a cylindrical jet interacting with a wind is observable within a larger solid angle.

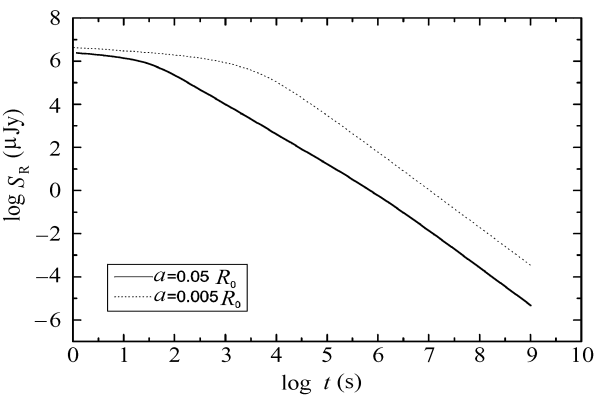

Fig. 4 R band afterglows from cylindrical jets without lateral expansion ($v_\perp \equiv 0$). The solid line and the dotted line correspond to cylindrical jets with $a = 0.05R_0$ and $a = 0.005R_0$, respectively. Other parameters are described in Section 3 of the main text. Note that the earlier light curve break here is produced by initial value effect, not by dynamics effect.

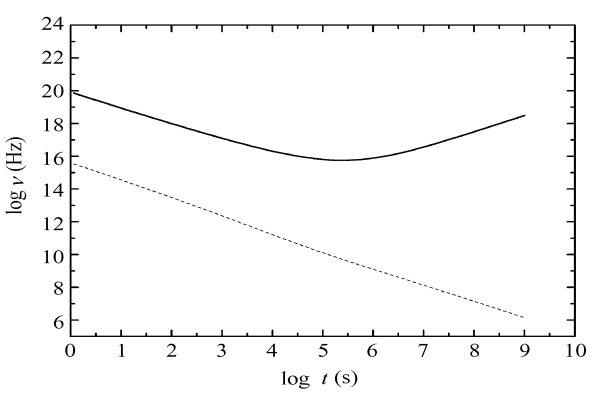

Fig. 5 Evolution of the cooling frequency $\nu_{\rm c}$ (solid line), and the peak frequency $\nu_{\rm m}$ (dashed line) in the case of $a = 0.05R_0$. Note that $\nu_{\rm R} = 4.37 \times 10^{14}$ Hz.

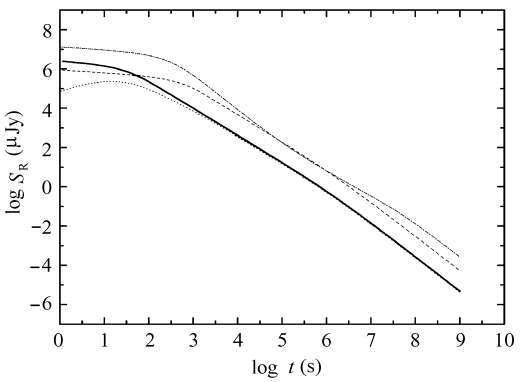

Fig. 6 Effect of ξ_e, ξ_B^2 and Θ on the R band light curve ($v_\perp \equiv 0$ case). The solid line is for $\xi_e = 0.1$, $\xi_B^2 = 10^{-6}$ and $\Theta = 0$. Each of the other lines has only one parameter altered with respect to the solid line. The dashed, dash-dotted and dotted lines correspond to $\xi_e = 0.5$, $\xi_B^2 = 10^{-4}$ and $\Theta = 0.1$ respectively. Other parameters not mentioned here are described in Section 3 of the main text.

3.2 The Case $v_\perp \equiv c_s$

In the $v_\perp \equiv c_s$ case, i.e. where the jet expands laterally at the comoving sound speed, deceleration surely occurs as the jet's cross section expands with radius. There are no simple power law relations between γ and t during the ultra relativistic phase, so no analytical solutions can be derived for the light curve. In the non-relativistic phase, $\gamma \sim 1$, $\beta \ll 1$, $c_s \approx \sqrt{5}\beta c/3$, and the dynamical equations reduce to

$$\frac{\mathrm{d}\beta}{\mathrm{d}m} \approx -\frac{\beta}{2m}, \quad \frac{\mathrm{d}m}{\mathrm{d}R} \approx \pi a^2 A R^{-2} m_p, \quad \frac{\mathrm{d}a}{\mathrm{d}t} \approx \frac{\sqrt{5}\beta c}{3}, \quad \frac{\mathrm{d}R}{\mathrm{d}t} \approx \beta c. \tag{9}$$

The solution is easy to obtain: $\beta \propto m^{-1/2}$, $a \propto R$, $m \propto R$, so we can derive

$$m \propto t^{2/3}, \quad \beta \propto t^{-1/3}, \quad R \propto t^{2/3}, \quad a \propto t^{2/3}. \tag{10}$$

Then we have $e' \propto (\gamma - 1)R^{-2} \propto t^{-2}$, $B' \propto (e')^{1/2} \propto t^{-1}$, $\nu_c \propto \gamma\gamma_c^2 B' \propto t$, $\nu_m \propto \gamma\gamma_{e,\min}^2 B' \propto t^{-1}$, $S_{\nu,\max} \propto \gamma N_e B' \propto t^{-1/3}$. So the flux density is

$$S_\nu \approx \begin{cases} S_{\nu,\max}\left(\frac{\nu}{\nu_m}\right)^{-(p-1)/2} \propto \nu^{-(p-1)/2} t^{-(3p-1)/6}, & (\nu_m \le \nu < \nu_c, \ \text{slow cooling}), \\ S_{\nu,\max}\left(\frac{\nu_c}{\nu_m}\right)^{-(p-1)/2}\left(\frac{\nu}{\nu_c}\right)^{-p/2} \propto \nu^{-p/2} t^{-(3p-4)/6}, & (\nu_m < \nu_c \le \nu, \ \text{slow cooling}), \\ S_{\nu,\max}\left(\frac{\nu}{\nu_c}\right)^{-1/2} \propto \nu^{-1/2} t^{1/6}, & (\nu_c \le \nu < \nu_m, \ \text{fast cooling}), \\ S_{\nu,\max}\left(\frac{\nu_m}{\nu_c}\right)^{-1/2}\left(\frac{\nu}{\nu_m}\right)^{-p/2} \propto \nu^{-p/2} t^{-(3p-4)/6}, & (\nu_c < \nu_m \le \nu, \ \text{fast cooling}). \end{cases} \tag{11}$$

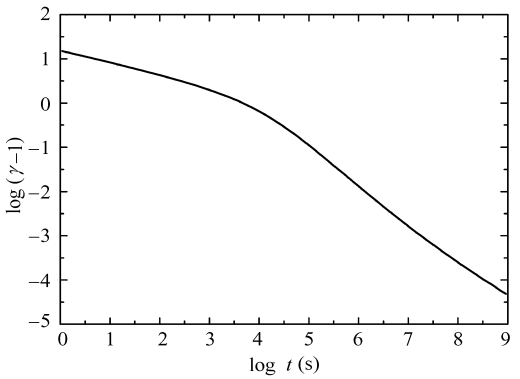

Fig. 7 Evolution of the Lorentz factor, γ, when $v_\perp \equiv c_{\rm s}$.

Figure 7 illustrates the evolution of γ when lateral expansion is present. We can see the jet become Newtonian after $t \approx 10^4$ s. The light curve of the R-band afterglow turns flatter in the Newtonian phase (see Fig. 8), which is quite different from the conical jet (Gou et al. 2001a, b). From the above we know that we can only derive the slope in the "flat" stage as $-(3p-1)/6$. When p is 2.5, the slope is -1.05, consistent with the theoretical result -1.08. In the earlier part of the light curve the slope is about -2.3. Figure 9 illustrates the impact on the light curve of three other parameters, $\xi_{\rm e}$, $\xi_{\rm B}^2$ and Θ.

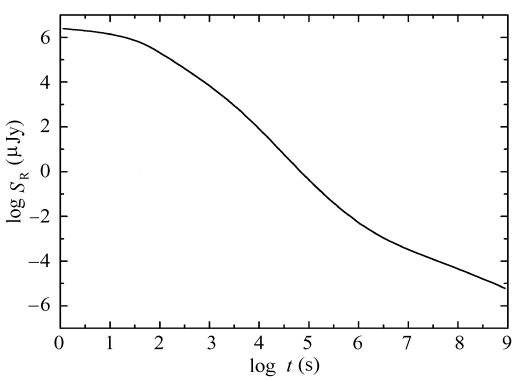

Fig. 8 R band afterglows from cylindrical jets with lateral expansion ($v_\perp \equiv c_{\rm s}$). All parameters are described in Section 3 of the main text. Note that the cylindrical jets here are already non-relativistic when $t > 10^4$ s.

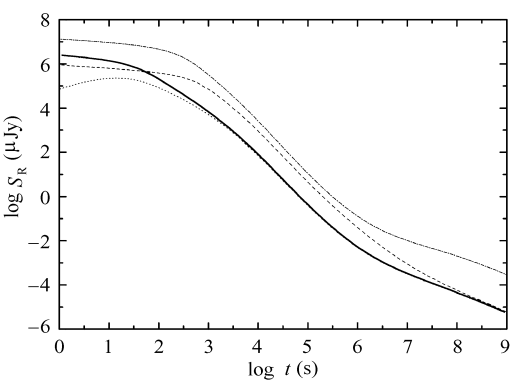

Fig. 9 Effect of $\xi_{\rm e}$, $\xi_{\rm B}^2$ and Θ on the R band light curve ($v_\perp \equiv c_{\rm s}$ case). The solid line is for $\xi_{\rm e} = 0.1$, $\xi_{\rm B}^2 = 10^{-6}$ and $\Theta = 0$. Each of the other lines has only one parameter altered with respect to the solid line. The dashed, dash-dotted and dotted lines correspond to $\xi_{\rm e} = 0.5$, $\xi_{\rm B}^2 = 10^{-4}$ and $\Theta = 0.1$ respectively. Other parameters not mentioned here are described in Section 3 of the main text.

4 DISCUSSION AND CONCLUSIONS

CHL has considered dynamical evolution of cylindrical jets in a homogeneous external medium and discussed their afterglows. Comparing our light curves with CHL's, we can see that the light curves are steeper when cylindrical jets interact with the wind. It is argued that some GRBs with $S_\nu \propto t^{-1.1}$— $t^{-1.3}$, such as GRBs 970508, 971214, 980329 and 980703, may be due to cylindrical jets without lateral expansion, and that they may not necessarily be due to isotropic fireballs (Huang et al. 2002). Some optical emission of afterglows had a steeper than usual decline. For example, GRB 970228 decayed as $t^{-1.7}$ after the subtraction of an underlying

supernova emission (Reichart 1999; Galama et al. 2000). The light-curve of GRB 980326 fell off as $t^{-2.1}$ (Groot et al. 1998), which also showed a supernova contribution (Bloom et al. 1999). A t^{-2} decay was observed for the afterglow of GRB 980519 (Halpern et al.1999). Price et al. (2002) compared several models and found that the isotropic wind model is the only model to interpret the optical afterglow of GRB 011121, whose light-curve decayed as $t^{-1.66}$. Chevalier & Li (1999) interpreted these steeper declines as isotropic fireballs interacting with pre-ejected winds and with an electron index around 3. We make the reasonable assumption that optical afterglows follow the standard power-law model, $S_\nu \propto t^{-\alpha}\nu^{-\beta}$. If $\nu_{\rm m} < \nu_{\rm R} < \nu_{\rm c}$, then in CL's model $\alpha = 3\beta/2 + 1/2$, while in our model $\alpha = \beta + 1$. We set up a table to compare our model with CL's model. From Table 1, we can see that cylindrical jets without lateral expansion in wind environments can also interpret these afterglows with steeper declines.

Table 1

Afterglow	α	β	$\alpha - 3\beta/2 - 1/2$	p	$\alpha - \beta - 1$	p	Reference
GRB 970228	$1.73^{+0.09}_{-0.12}$	0.78 ± 0.02	0.06	2.64	-0.05	2.46	Galama et al. (2000)
GRB 980326	2.0 ± 0.1	0.8 ± 0.4	0.3	3.0	0.2	3.0	Bloom et al. (1999)
GRB 980519	2.05 ± 0.04	1.20 ± 0.25	-0.25	3.07	-0.15	3.10	Halpern et al. (1999)
GRB 011121	1.66 ± 0.06	0.76 ± 0.15	0.02	2.55	-0.10	2.32	Price et al. (2002)

$S_\nu \propto t^{-\alpha}\nu^{-\beta}$, both α and β depend on the electron energy distribution index, p. $\alpha - 3\beta/2 - 1/2$ shows how well the CL's model fits the light curves of these afterglows, and values of the first p are obtained by α from this model, i.e. $\alpha = (3p-1)/4$. $\alpha - \beta - 1$ has the same meaning as $\alpha - 3\beta/2 - 1/2$ but for cylindrical jets in winds, where $\alpha = (p+1)/2$.

Most progenitor models of GRB involve either the cataclysmic collapse of a massive rotating star into a black hole, or a neutron star merging with a black hole or another neutron star (Woosley 1993; MacFadyen & Woosley 1999; Paczyński 1986; Zhang, Woosley & MacFadyen 2002). Because the material accreting into the black hole forms a rotating disk, it blocks the outflow of mass, so any material that does escape is forced into two narrow and oppositely directed jets. Considering this, we can say cylindrical jets may be more realistic to interpret afterglows than isotropic fireballs. If GRBs are really due to cylindrical jets, they can be easily produced by a supernova-like event (CHL).

Observations of relativistic outflows in radio galaxies reveal that lateral expansion is unobtrusive, and a jet usually maintains a constant cross-section at large scales (Perley et al. 1984; Biretta et al. 1999). This is perhaps due to magnetic confinement and/or external pressure. So lateral expansion may take effect only when the jets are far away from the progenitors, where perhaps the circumstance is not a wind any more. We can see, in the case of narrow cylindrical jets, jets whose light curves are fitted by ISM circumstance can originate from massive stars, but they pass across the wind regions in hundreds or thousands of seconds.

Acknowledgements We thank B. Zhang for helpful suggestion. This work was supported by The Foundation for the Author of National Excellent Doctoral Dissertation of P. R. China (Project No: 200125), the Special Funds for Major State Basic Research Projects, the National Natural Science Foundation of China, and the National 973 Project (NKBRSF G19990754).

References

Akerlof C., Balsano R., Barthelmy S. et al., 1999, Nature, 398, 400
Biretta J. A., Sparks W. B., Macchetto F., 1999, ApJ, 520, 621
Blandford R. D., McKee C. F., 1976, Phys. Fluids, 19, 1130
Bloom J., Kulkarni S. R., Djorgovski S. G. et al., 1999, Nature, 401, 453
Cheng K. S., Lu T., 2001, Chinese J. Astron. Astr., 1, 1
Cheng K. S., Huang Y. F., Lu T., 2001, MNRAS, 325, 599 (CHL)
Chevalier R. A., Li Z. Y., 1999, ApJ, 520, L29 (CL)
Chevalier R. A., Li Z. Y., 2000, ApJ, 536, 195
Dai Z. G., Huang Y. F., Lu T., 1999, ApJ, 520, 634
Dai Z. G., Lu T., 1998, MNRAS, 298, 87
Dai Z. G., Lu T., 1999, ApJ, 519, L155
Galama T., Tanvir N., Vreeswijk P. M. et al., 2000, ApJ, 536, 185
Ghisellini G. 2001, Invited talk at the 25th Johns Hopkins Workshop: "2001: A Relativistic Spacetime Odyssey. Experiments and Theoretical Viewpoints on General Relativity and Quantum Gravity", Florence (astro-ph/0111584).
Gou L. J., Dai Z. G., Huang Y. F., Lu T., 2001a, Chin. Astron. Astr., 25, 29
Gou L. J., Dai Z. G., Huang Y. F., Lu T., 2001b, A&A, 368, 464
Halpern J., Kemp J., Piran T., Bershady M., 1999, ApJ, 517, L105
Huang W. G., Yang P. B., Lu Y., 2001, Chin. Astron. Astr., 25, 291
Huang Y. F., Dai Z. G., Lu T., 1998, Chin. Phys. Lett., 15, 775
Huang Y. F., Dai Z. G., Lu T., 1999a, Chin. Phys. Lett., 16, 775
Huang Y. F., Dai Z. G., Lu T., 1999b, MNRAS, 309, 513
Huang Y. F., Gou L. J., Dai Z. G., Lu T., 2000a, ApJ, 543, 90
Huang Y. F., Dai Z. G., Lu T., 2000b, MNRAS, 316, 943
Huang Y. F., Dai Z. G., Lu T., 2000c, Chin. Phys.Lett., 17, 778
Huang Y. F., 2000, preprint, astro-ph/0008177
Huang Y. F., Tan C. Y., Dai Z.G., Lu T., 2002, Chin. Astron. Astr., 26, 414
Katz J. I., 1994, ApJ, 422, 248
Kobayashi S., Zhang B., 2003, ApJ, 582, L75
MacFadyen A., Woosley S. E., 1999, ApJ, 524, 262
MacFadyen A., Woosley S. E., Heger A., 2001, ApJ, 550, 410
Mao J. R., Wang J. C., 2001a, Chin. J. Astron. Astr., 1, 349
Mao J. R., Wang J. C., 2001b, Chinese J. Astron. Astr., 1, 433
Mészáros P., Rees M. J., 1997, ApJ, 476, 232
Paczyński B., 1986, ApJ, 308, L43
Paczyński B., 1998, ApJ, 494, L45
Perley R. A., Bridle A. H., Willis A. G., 1984, ApJS, 54, 2910
Price P. A., Berger E., Reichart D. E. et al., 2002, ApJ, 572, L45
Rees M. J., Mészáros P., 1992, MNRAS, 258, L41
Reichart D., 1999, ApJ, 521, L111
Rhoads J. E., 1997, ApJ, 478, L1
Rybicki G. B., Lightman A.P., 1979, Radiative Processes in Astrophysics, New York: Wiley
Sahu K. C., Livio M., Petro L. et al., 1997, Nature, 387, 476
Sari R., Piran T., Narayan R., 1998, ApJ, 497, L17
van Paradijs J. P., Groot P. J., Galama T. et al., 1997, Nature, 386, 686
Willis A. J., 1991, In: K. A. van der Hucht, B. Hidayat, eds., IAU Symp. 143, Wolf-Rayet Stars and Interrelations with Other Massive Stars in Galaxies, Dordrecht: Kluwer, 265
Woosley S., 1993, ApJ, 405, 273
Wu M., Tang S. K., Zhang P. et al., 2001, Sci. China Ser. A, 44, 1608
Zhang B., Mészáros P., 2002, ApJ, 581, 1236
Zhang W., Woosley S.E., MacFadyen A., 2002, A&AS, 200, 3213